

<b>LAM</b> <b>LOOM</b>	Projet	REF: <b>LOOM.KD.SPIRE.2000.002-4</b>	PAGE: 1 / 24
	<b>SPIRE</b>	Author : <b>Kjetil Dohlen</b>	Date: <b>17 Jan 2002</b>
<b>Herschel - SPIRE: Optical Error Budgets</b>			

**SPIRE-LAM-PRJ-000446**

<b>RAL</b>	K.King			
	B.Swinyard	<b>X</b>		
<b>CNES</b>	M.Joubert		Y.Blanc	
<b>CEA-Sap</b>	Jean-Louis Auguères			
<b>LAS</b>	J.P.Baluteau	<b>X</b>	D. Ferrand	
	K.Dohlen	<b>X</b>	R. Malina	
	A.Origné	<b>X</b>	P.Dargent	<b>X</b>
	D.Pouliquen	<b>X</b>		

## Updates

<b>Date</b>	<b>Indice</b>	<b>Remarks</b>
22 May 2000	DRAFT	Creation of the document
30 June 2000	1	First release
5 December 2000	2	Exact sized photometer cold stop. Focus budget
22 August 2001	3	Telescope name changed. Baseline systems updated. Telescope and focus added to wavefront budgets. Telescope alignment included in Phot pupil alignment budget. Pupil alignment added in Spec throughput budget. Fringe contrast calculations revised for clipped Gaussian.
17 January 2002	4	Discussion of statistics (sec. 2.2). External alignment of RD5 (sec. 3.2.1 and 3.3.1). Longitudinal position and azimuthal rotation considered (sec 3.3.1). RT replaces CC. Instrument external budget increased.

## Reference documents

<b>#</b>	<b>Title</b>	<b>Author(s)</b>	<b>Reference</b>	<b>Date</b>
1	FIRST alignment plan		PT-PL-02220	9/5/96
2	"Martin-Puplett interferometer: an analysis"	Lambert, Richards	Applied Optics 17, 1595 (1978)	1978
3	Filters, Beam Splitters & Dichroics	P.A.R. Ade, C.E Tucker M.J. Griffin, P.C.Hargrave	SPIRE Preliminary Design Review	7-9 July 1999
4	"The calculation of image quality", p.225	W. B. Wetherell	Appl. Opt. and Opt. Eng., vol VIII, Eds R. R. Shannon, J. C. Wyant, Academic Press, London	1980
5	"Herschel Alignment Concept	D. Schink	HP-2-ASED-TN-0002	12/07/01

File	ErrorBudgetsV4_01.DOC
Printed	25/01/02 11:52

## 1. Scope

This document presents optical error budgets for SPIRE.

### 1.1. Table of contents

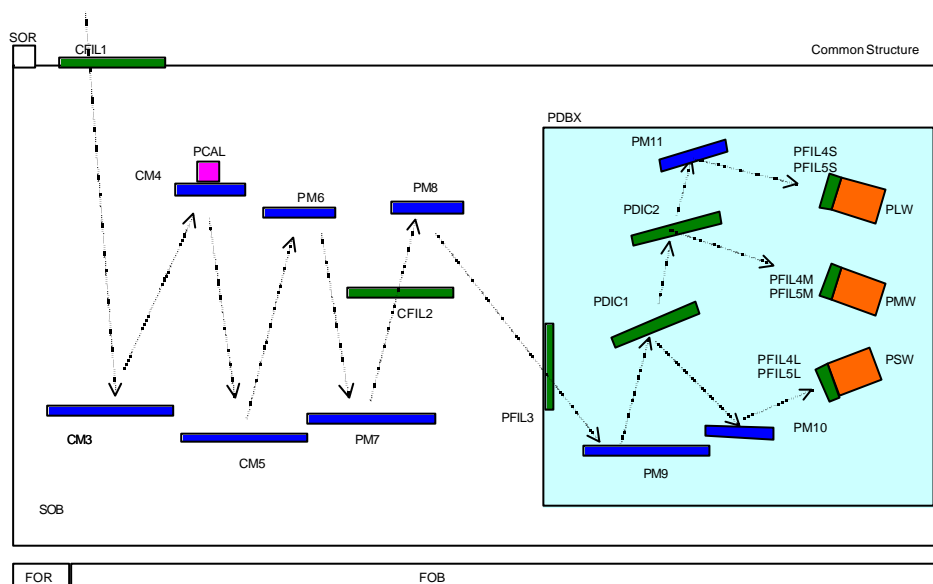
<b>1. Scope .....</b>	<b>3</b>
<i>1.1. Table of contents.....</i>	<i>3</i>
<b>2. Introduction .....</b>	<b>4</b>
<i>2.1. Baseline designs.....</i>	<i>4</i>
<i>2.2. Statistical considerations.....</i>	<i>5</i>
<i>2.3. One-dimensional statistics .....</i>	<i>5</i>
<b>3. Photometer budgets .....</b>	<b>7</b>
<i>3.1. Throughput.....</i>	<i>7</i>
<i>3.2. Wavefront error.....</i>	<i>8</i>
3.2.1. Defocus contributions .....	8
3.2.2. Mirror fabrication .....	8
3.2.3. Internal alignment.....	9
<i>3.3. Pupil alignment.....</i>	<i>11</i>
3.3.1. Telescope to SPIRE interface .....	11
3.3.2. Instrument external alignment.....	13
3.3.3. Instrument internal alignment.....	13
<b>4. Spectrometer budgets.....</b>	<b>16</b>
<i>4.1. Throughput.....</i>	<i>16</i>
<i>4.2. Wavefront error.....</i>	<i>17</i>
<i>4.3. Interferogram contrast.....</i>	<i>18</i>
4.3.1. Wavefront tilt .....	18
4.3.2. Wavefront shear.....	19
4.3.3. Optical design .....	20
4.3.4. Interferometer alignment.....	21
4.3.5. Beamsplitter balance.....	23
4.3.6. Budget .....	24

## 2. Introduction

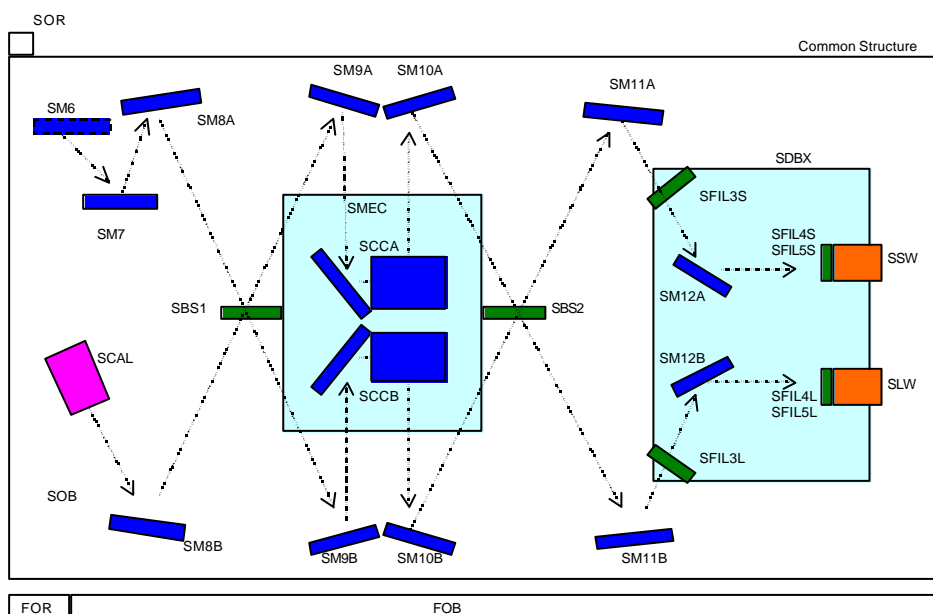
Optical error budgets for the SPIRE instruments are presented. Throughput and wavefront error (Strehl ratio) budgets are presented for both photometer and spectrometer channels. Alignment tolerances are considered by way of a pupil alignment budget for the photometer and an interferogram contrast budget for the spectrometer.

### 2.1. Baseline designs

Current baselines are BOLPHT155D for the photometer channel and BOLSP508 for the spectrometer channel. Schematic representations of the systems with symbolic names for each component are shown in Figure 1.



(a)



(b)

Figure 1. Schematic layout of the photometer channel (a) and spectrometer channel (b) of the SPIRE instrument.

<b>LAM</b> <b>LOOM</b>	<b>Projet</b> <b>SPIRE</b>	Herschel - SPIRE: Optical Error Budgets REF : LOOM.KD.SPIRE.2000.002-4	PAGE : 5 / 24 17 Jan 2002
---------------------------	-------------------------------	---	------------------------------

## 2.2. Statistical considerations

Most of the budgets are based on root-sum squaring (RSS) in order to estimate total instrument performance. The RSS operation has different significance in different cases:

- **Wavefront error:** If the optical surfaces have random and mutually independent wavefront errors (WFE), then the total RMS error equals the RSS sum of the individual contribution.
- **1-D errors:** If a performance criterion is given as the algebraic sum of errors for a large number of components, then the RSS sum of the tolerances for each component has statistical significance for the expectable system performance.
- **2-D errors:** If a performance criterion is the length of a vector with two (or more) dimensions (e.g. the position of a ray impact on a surface), then the position error is the RSS sum of the errors along each dimension.

In the wavefront error budgets presented in this note, the first case concerns mirror fabrication errors, while focus errors are governed by the second case. In the alignment budgets, cases two and three are encountered.

The first and third cases are determinate. As long as each individual error is below the specified value, the total performance is better than the budget total. In the second case, there is a certain probability that the total performance is worse than the budget. We discuss here the validity and statistical significance of this approach.

## 2.3. One-dimensional statistics

We assume a one-dimensional performance parameter  $x$  (e.g. the x-component of the position of the instrument pupil as projected onto the telescope pupil) as the sum of  $N$  individual component performances,  $x_i$ :

$$x = \text{Sum}(x_i)$$

If each  $x_i$  is governed by Gaussian statistics with standard deviation  $\sigma_i$ , then  $x$  also has a Gaussian probability distribution with standard deviation  $\sigma$ , given by:

$$\sigma = \text{Sqrt}(\text{Sum}(\sigma_i^2)) = \text{RSS}(\sigma_i).$$

If each component performance is related directly to a manufactured piece, such as a mirror stand, it may be expected to have a square probability distribution rather than a Gaussian one. That is, it has an even probability of being anywhere within a tolerance range  $\pm a_i$ . The standard deviation of a square distribution is given by

$$\sigma_i = a_i/\sqrt{3}.$$

The sum of a series of square-distribution parameters has a statistical distribution close to that of a Gaussian (see figure), and, as we may expect, its standard deviation is the RSS of that of each component:

$$\sigma = \text{RSS}(\sigma_i) = \text{RSS}(a_i)/\sqrt{3}.$$

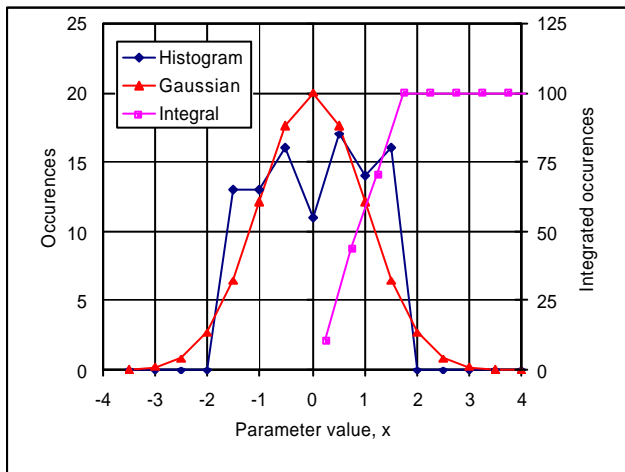
Hence, if a budget gives tolerances  $a_i$  for each component, then the top-level RSS budget represents the  $\sqrt{3}\sigma$ -level for the system performance:

$$\text{RSS}(a_i) = \sqrt{3} \sigma.$$

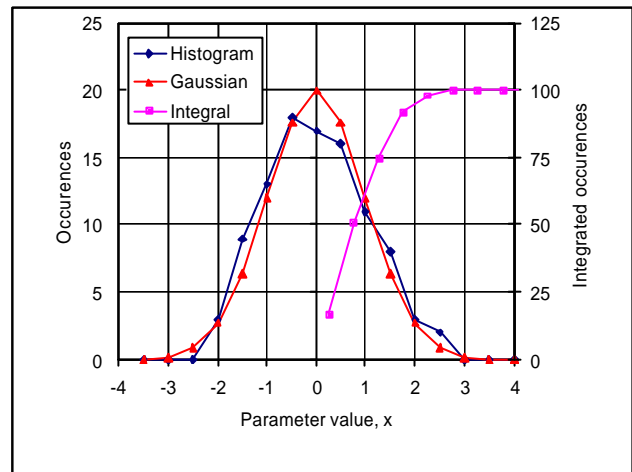
If the performance parameter has a Gaussian distribution and its optimal value is zero, then the probability of finding a value within the range  $\pm x$  is given by integrating the Gaussian function from  $-x$  to  $x$ . The table below gives some values for the Gaussian (normalized to unity at its peak) and of this integral (normalized to unity at infinity).

x	Gaussian	Integrated Gaussian
0	1	0
$\sigma$	61%	68%
$\sqrt{3} \sigma = 1.73 \sigma$	22%	92%
$2 \sigma$	14%	96%
$3 \sigma$	1.1%	99.7%

The left-hand panel of the figure shows the histogram of 100 realisations of a single, square-distribution parameter whose tolerance is  $a = \sqrt{3}$ , compared with a Gaussian distribution with  $\sigma = 1$ . In the right-hand panel, the histogram of 100 realisations of the sum of 10 square-distribution parameters, each with a tolerance of  $a_i = \sqrt{(3/10)} = 0.548$ , again compared with a Gaussian distribution with  $\sigma = 1$ . The integrated probability is also shown in each case.



Histogram (blue) of a single square-distribution parameter compared with a Gaussian (red). Integrated probability (violet) on the right-hand axis.



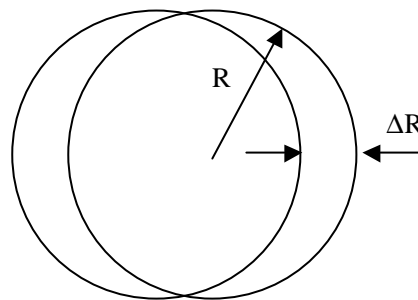
Histogram (blue) of the sum of 10 square-distribution parameters compared with a Gaussian (red). Integrated probability (violet) on the right-hand axis

The assumptions taken for the current budget therefore ensures a 92% probability of reaching the required performance. To reach a near-100% certainty, usually assumed by the  $3\sigma$  criterion, individual tolerances must be nearly halved. This seems to be unjustified for the internal instrument alignment where actual performance will be measured and an adjustment possibility exists (machining the M6 stands). However, the  $3\sigma$  criterion may be justified for the external alignment between instrument and telescope for which no possibility for performance verification and adjustment exists. In that case, we must insist that the telescope manufacturer uses  $3\sigma$  values in his alignment budget.

### 3. Photometer budgets

#### 3.1. Throughput

Apart from filters and dichroics, major part of budget is due to sizing of cold stop. Undersizing was originally assumed, but it has been proven acceptable to use exact sizing of the cold stop. This means that the cold stop within the SPIRE instrument is given the dimensions of the geometrical image of the telescope pupil (M2). Due to variations in the pupil image for different points in the FOV (pupil aberrations) and instrument misalignments (see alignment budget, Sec. 3.3), the cold stop will not be exactly aligned with the telescope pupil, however, resulting in a loss of throughput. This loss has been estimated by considering the common area of displaced circles, see Figure below.



The transmission of the resulting system equals the fraction of the overlapping area ( $A$ ) to the pupil area ( $A_0$ ). With analogy to the calculation of optical MTF (see sec. 4.3.2), this fraction may be given by the approximation:

$$\frac{A}{A_0} \approx 1 - \frac{4}{p} u = 1 - \frac{2\Delta R}{pR} = 1 - 0.64 \frac{\Delta R}{R}$$

where  $\Delta R/R$  is the fractional displacement between the two circles.

Diffraction and baffling losses have been estimated to 20% (TBC). Reflection efficiency assume a reflectivity of 99% per surface for 8 mirror surfaces. Total filter and dichroic transmission has been assumed to be within the specified 40%.

Horn coupling efficiency is not included.

Current throughput budget (see Fig 2) is in accordance with the IRD requirement.

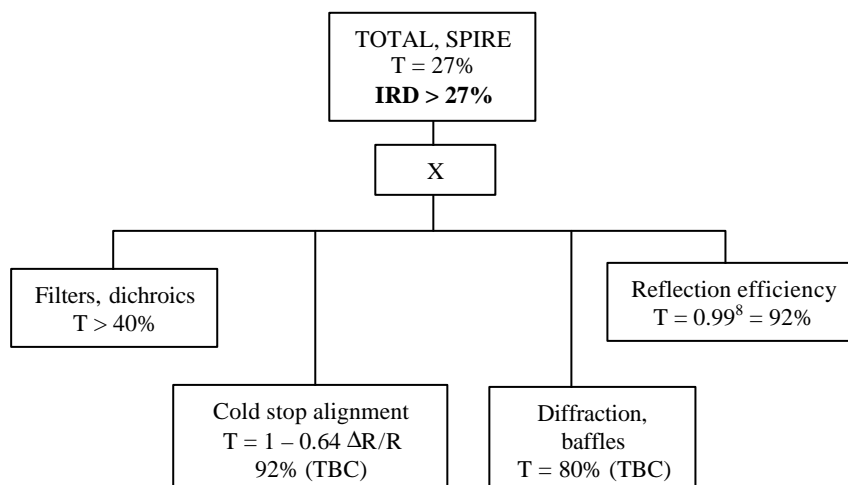


Figure 2. Photometer throughput budget.

### 3.2. Wavefront error

Figure 3 shows the budget of root mean square wavefront errors (WFErms) for the SPIRE photometer including telescope. It is divided into three main parts: SPIRE instrument, the telescope system, and external alignments. Astrium is responsible for both telescope and external alignment, but the error budget provided by Astrium France (Matra) for the telescope (view graphs from Working meeting at ESTEC 19 June 2001) does not appear to include the alignments between the telescope sub-system and the instruments. We include the defocus allocation given by Astrium in [RD5], see below.

Unless otherwise noted, the budget is obtained by RSS summing of individual contributions:

$$WFErms^2 = \sum_i WFErms_i^2$$

Focus errors and higher order aberrations are treated equally. Since the IRD requirement is given in terms of Strehl ratio, all wavefront errors are accompanied by their Strehl ratio equivalent calculated by the Marechal approximation at  $\lambda = 250 \mu\text{m}$ :

$$S \approx 1 - \frac{4p^2}{I^2} WFErms^2$$

#### 3.2.1. Defocus contributions

Wavefront error due to defocus  $\Delta z$  is given by:

$$WFErms = \frac{\Delta z}{16\sqrt{3}F^2}$$

At the telescope focus, with  $F = 8.68$ , this becomes  $WFErms [\mu\text{m}] = 0.48 \Delta z [\text{mm}]$ . At the instrument focus, with  $F = 5$ , we have  $WFErms [\mu\text{m}] = 1.44 \Delta z [\text{mm}]$ . None of the defocus contributions assumed in the SPIRE internal budget are significant. The external, telescope to instrument interface, focus alignment budget and its breakdown are assumed as defined in RD5. It is a significant contribution to the overall budget. Note that RD5 assumes RSS summing of the three components of its breakdown. This is risky since focus errors add linearly: the probability of being worse than the RSS value is high. **SPIRE therefore stresses that the interface requirements are given by the total external alignment budget and not by its individual components. Furthermore, the performance should either be verified by measurement, or guaranteed with a 3s (99.7%) certainty.**

#### 3.2.2. Mirror fabrication

The mirror fabrication budget has been separated into two parts, considering surface shape and radius of curvature separately. A specification on radius of curvature of  $\Delta R/R = 10^{-3}$  has been assumed for each surface. This may be translated into a wavefront error contribution per surface of

$$WFErms = \frac{h^2}{2\sqrt{3}R} \frac{\Delta R}{R}$$

where  $h$  is sub-pupil radius at the surface and  $R$  is nominal radius of curvature. Table 3.1 shows results of these calculations for each surface in the photometer optical train.

A WFErms of  $2 \mu\text{m}$  per reflecting surface (e,  $1 \mu\text{m}$  rms measured on the surface itself) has been assumed for each of 9 surfaces (CM3 to PM9 plus 1 dichroic plus 1 fold mirror). The total budget entry is:  $WFErms = \sqrt{9} \times 2 \mu\text{m} = 6 \mu\text{m}$ .

No contribution is assumed for transmissive components (filters and dichroics) since they are assumed to have negligible optical thickness.



### 3.2.3. Internal alignment

Internal alignment has been given very strict tolerances in order to ensure pupil alignment, as described in Sec. 3.3. The effect of alignment errors on the wavefront budget is therefore negligible. Additional allocations of 0.5 mm in axial alignment of detectors with respect to the instrument focal plane and the instrument with respect to the telescope focal plane have been given, but these are seen to be insignificant as well.

The IRD requirement of  $S > 0.9$ , corresponding to  $WFE_{rms} < 12.6 \mu m$ , is achieved with some margin.

*Table 3.1. Defocus wavefront error due to  $DR/R = 10^{-3}$  precision on radius of curvature for each surface*

<b>Mirror</b>	<b>R</b>	<b>h</b>	<b>DR</b>	<b>WFE<sub>rms</sub></b>
CM3	370	5.5	0.37	0.02
CM5	300	18	0.3	0.31
PM6	300	0.03	0.3	0.00
PM7	330	19	0.33	0.32
PM8	290	18	0.29	0.32
PM9	350	35	0.35	1.01
Total				1.15

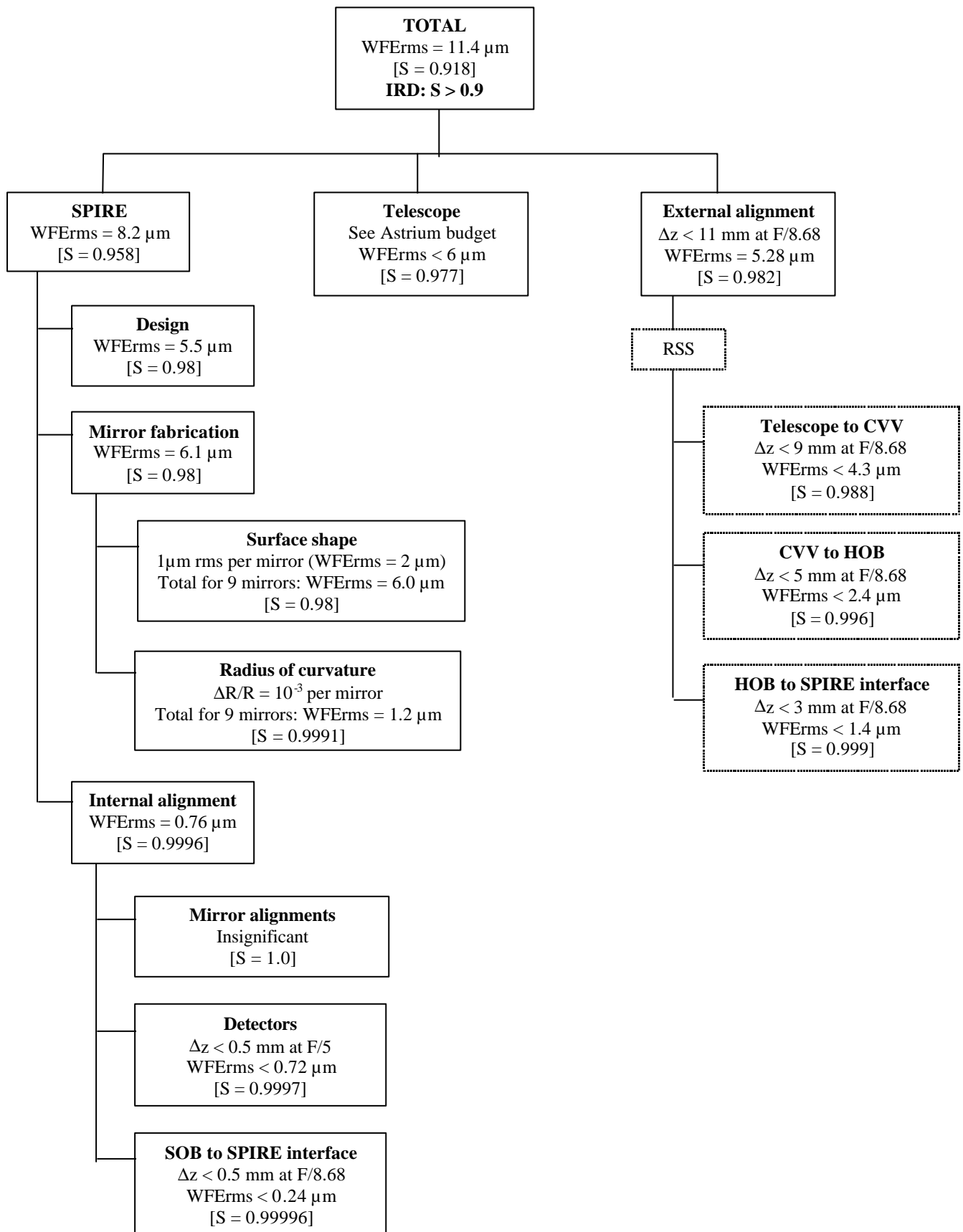


Figure 3. Photometer wavefront error budget.

<b>LAM</b> <b>LOOM</b>	<b>Projet</b> <b>SPIRE</b>	Herschel - SPIRE: Optical Error Budgets REF : LOOM.KD.SPIRE.2000.002-4	PAGE : 11 / 24 <b>17 Jan 2002</b>
---------------------------	-------------------------------	---	--------------------------------------

### 3.3. Pupil alignment

The pupil alignment budget (Fig. 4) is dimensioning for mechanical tolerances in the photometer case. There is no IRD on pupil alignment, but, as has been shown in the throughput budget (Fig. 2), it has a strong influence on instrument throughput.

The four major components of the budget are outlined in heavy lines in the figure: optical design, telescope alignment, instrument external alignment, and instrument internal alignment.

**Optical design** quantifies the variation in pupil position for different points in the FOV for a perfectly aligned instrument, due to pupil aberrations. We believe that this value has been minimized for the optical concept chosen, and that a further reduction would require important complications of the optical design.

**Telescope alignment** considers degradation of pupil alignment due to misalignments under ESA contractor control, i.e. alignment between the Herschel telescope and its optical bench, HOB, up to SPIRE fixation points.

**Instrument external** concerns alignment between instrument fixation points and the SPIRE optical bench (SOB). This includes in particular uncertainties linked to alignment verification procedures.

**Instrument internal** concerns alignment of optical components with the SOB.

The budget shows a good balance between these four components. The contributions from instrument internal and external alignment are the smallest, indicating some margin and that no great improvement can be expected from reducing the mechanical tolerance values.

*The two top budget components, design and alignment, are summed because the pupil aberrations are deterministic. All other components are "root-sum-squared".*

#### 3.3.1. Telescope to SPIRE interface

The original ESA alignment plan [RD1] was not clear on the alignment performance requirement between telescope and instrument. The new plan [RD5] does not clarify the situation, and clarification has been requested. For our budget we assume a total misalignment corresponding to a tilt of  $\delta\alpha = 12'$  at the instrument focus. Then the relative pupil alignment ( $\Delta R/R$ ) is given by:

$$\Delta R/R = \delta\alpha s / (D_{M2}/2) = 2 F \delta\alpha = 6\%,$$

where  $s$  is distance from M2 to focal surface,  $D_{M2}$  is M2 diameter, and  $F = s/D_{M2} = 8.68$  is the focal ratio. A break down of this budget is provided in [RD5] as reproduced in Table 3.2.

Table 3.2. Break down of Herschel telescope to instrument transverse alignment budget.  
Reproduced from [RD5].

Alignment Step	Axis (arcmin)	Lateral (mm)	ResultingTilt (arcmin)
Instrument adjustment w.r.t. OB 1)	8	3	9.11
OB w.r.t. CVV	1	0.5	1.2
Telescope knowledge	NA	1	1.5
PLM / Telescope adjustment	1	1	1.8
Telescope stability	NA	0.1	0.1
Instrument stability 2)			
$r$ (ISO type)	0.4	0.3	0.6
Total			9.5

Table 3.2-1: Summary of Lateral and Tilt Alignment Requirements

- 1) It is assumed that the instrument internal alignment accuracy does not contribute to this value. If this is true, remark 2) is also obsolete. TBC by Alcatel  
2) Included in instrument adjustment

Pupil alignment is also affected by longitudinal misalignment (defocus) and azimuthal rotation (roll). [RD5] gives tolerances for these types of errors, but the document does not appear to take their effects on pupil alignment into account. We have calculated the effects of these errors and added them to the budget tree. Their participation to the overall budget are insignificant.

### 3.3.1.1 Transverse errors, tilt and decenter

We assume tilts ( $\delta\alpha$ ) around the centre of the SPIRE photometer FOV. Relative pupil displacement is given by ( $F = 8.68$ ):

$$\Delta R/R = 2 F \delta\alpha$$

so that, for  $F = 8.68$ :

$$\Delta R/R [\%] = 0.51 \delta\alpha [\text{arcmin}]$$

Decentering errors are directly equal to pupil decenters. Relative pupil displacement is therefore given by:

$$\Delta R/R = \Delta x / (D_{M2}/2) = 2 \Delta x / D_{M2}$$

so that, for  $D_{M2} = 308.1\text{mm}$

$$\Delta R/R [\%] = 0.65 \Delta x [\text{mm}]$$

Equating these two expressions gives an expression for the equivalence between tilt and decentering errors:

$$\delta\alpha [\text{arcmin}] = 1.29 \Delta x [\text{mm}].$$

**This expression is not consistent with the data reproduced in Table 3.2.**

<b>LAM</b> <b>LOOM</b>	<b>Projet</b> <b>SPIRE</b>	Herschel - SPIRE: Optical Error Budgets REF : LOOM.KD.SPIRE.2000.002-4	PAGE : 13 / 24 17 Jan 2002
---------------------------	-------------------------------	---	-------------------------------

### 3.3.1.2 Longitudinal errors, focus

We assume displacements of the instrument box along the telescope axis. In addition to wavefront error, this introduces field dependent pupil alignment errors. We calculate the effect at the edge of the unvignetted FOV of Herschel.

The principal rays from two points in the instrument focal plane converge at an angle  $\alpha$  and intersect in the instrument exit pupil (nominally M2). If M2 moves longitudinally a distance  $\Delta z$  with respect to this pupil, then the two beams intersect in two points separated by:

$$\Delta x = \Delta z \alpha.$$

By the Lagrange invariant, the angle  $\alpha$  is related to the field angle  $\beta$  projected on the sky by  $\alpha = \beta D_{M1}/D_{M2}$ , where the D represent telescope entrance and exit diameters, respectively.

Relative pupil misalignment as defined above is therefore:

$$\Delta R/R = \Delta x/(D_{M2}/2) = 2 \Delta z \beta D_{M1}/(D_{M2})^2.$$

Using  $D_{M1} = 3283$  mm,  $D_{M2} = 308.12$  mm and  $\beta = 0.25$  deg, we get

$$\Delta R/R [\%] = 0.03 \Delta z [\text{mm}].$$

For  $\Delta z = 11$  mm we get 0.3% relative pupil misalignment.

### 3.3.1.3 Azimuthal rotation

The effect of a rotation of the instrument around a vertical axis depends upon the distance of this axis from the telescope optical axis. Rotation around the telescope axis has no influence on the pupil alignment since chief rays from all points in the instrument FOVs converge on this point.

Rotation about the centre of the photometer FOV is a conservative estimation of the effects of rotations about the forward instrument foot. Rotation angle  $\phi$  produces a displacement  $\Delta x$  of the centre of the instrument exit pupil from the centre of M2:  $\Delta x = l \phi$ , where  $l$  is the distance from the telescope axis to the rotation axis. Hence, for relative pupil displacement:

$$\Delta R/R = \Delta x/(D_{M2}/2) = 2 l \phi/D_{M2}$$

With  $l = 91$  mm and  $\phi$  in degrees,  $\Delta R/R = 0.010 \phi$ . A 1 deg rotation therefore produces a 1% relative pupil alignment error.

## 3.3.2. Instrument external alignment

Instrument external alignment concerns alignment between instrument fixation points on the Herschel optical bench and the SPIRE optical bench (SOB). This includes in particular uncertainties linked to alignment verification procedures and components (cubes), but also fabrication tolerances for the feet and their connection to the SOB. This part of the budget has now been extracted from the instrument internal budget and its size has been increased, but only within the limit of sensitivity of the instrument throughput budget.

## 3.3.3. Instrument internal alignment

The instrument alignment budget concerns interfaces between SOB and optical components (mirrors and cold-stop). Mechanical tolerances have been set to 0.1 mm decenter for each component along each direction  $x$ ,  $y$ ,  $z$  and 1 arcmin tilt for each component around each axis. The effect of misalignments equal to these values for each component and each axis are obtained from a sensitivity analysis, summarized in Figure 5 (BolPhtRev05.mac, SpirePhotTol18.xls). Verification of the effect of random distributions of alignment errors is shown by the histogram plot of Figure 6 (SpirePhotTol20.xls).

*These tolerances should in each case be distributed on the required intermediate interfaces. For example, the CS is mounted on the 2K box which is in turn mounted on the SOB.*

Note that the components following the cold stop (PM9, folds, dichroics) have no influence on the CS alignment budget. Also, filters are not included since their thickness, and hence beam deviation, is negligible (TBC PA).

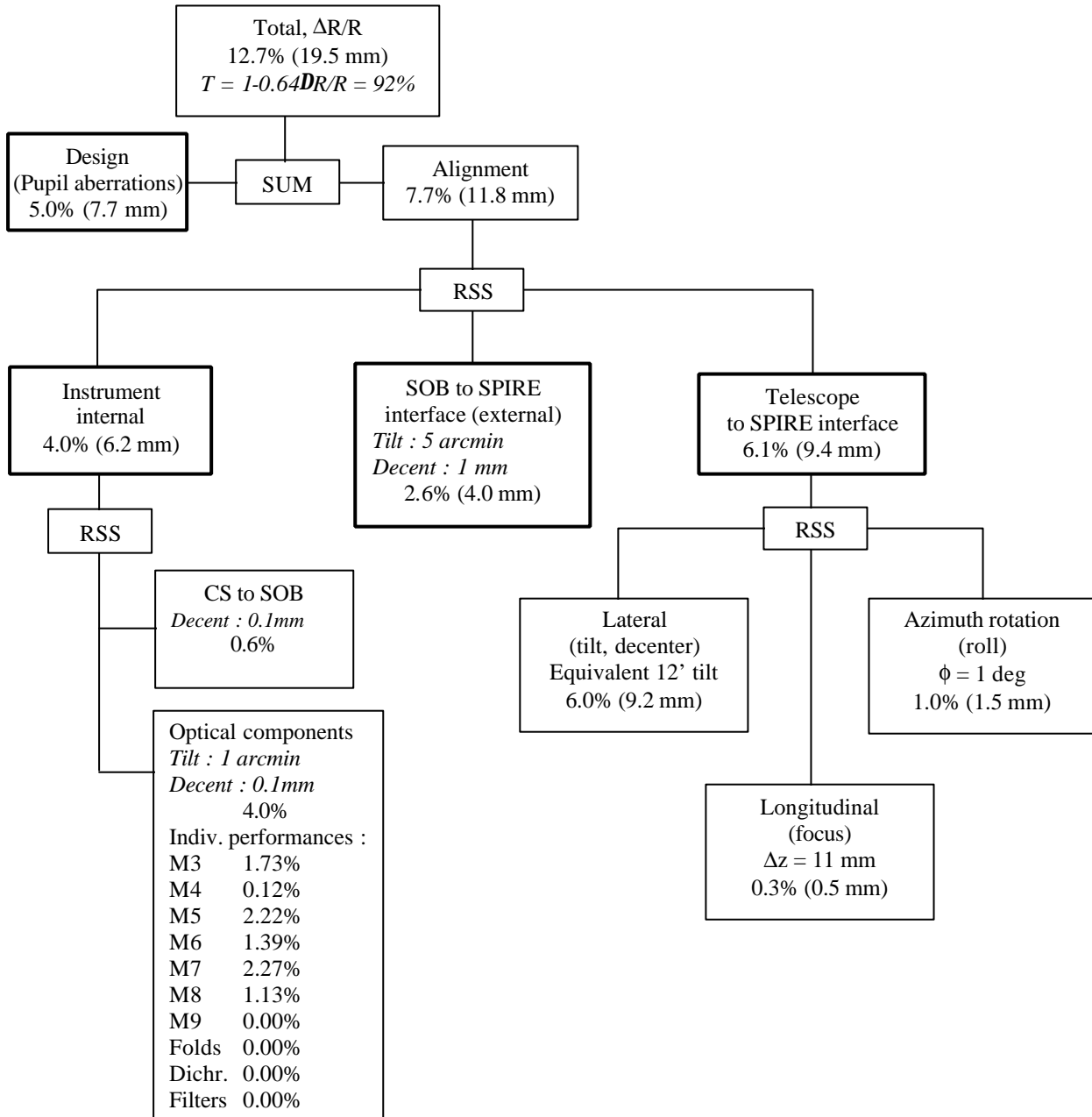


Figure 4. Pupil alignment budget for the photometer. The heavy boxes indicate the major components of the budget: optical design (pupil aberrations) telescope alignment under ESA responsibility, SPIRE intrnal and SPIRE external alignment.

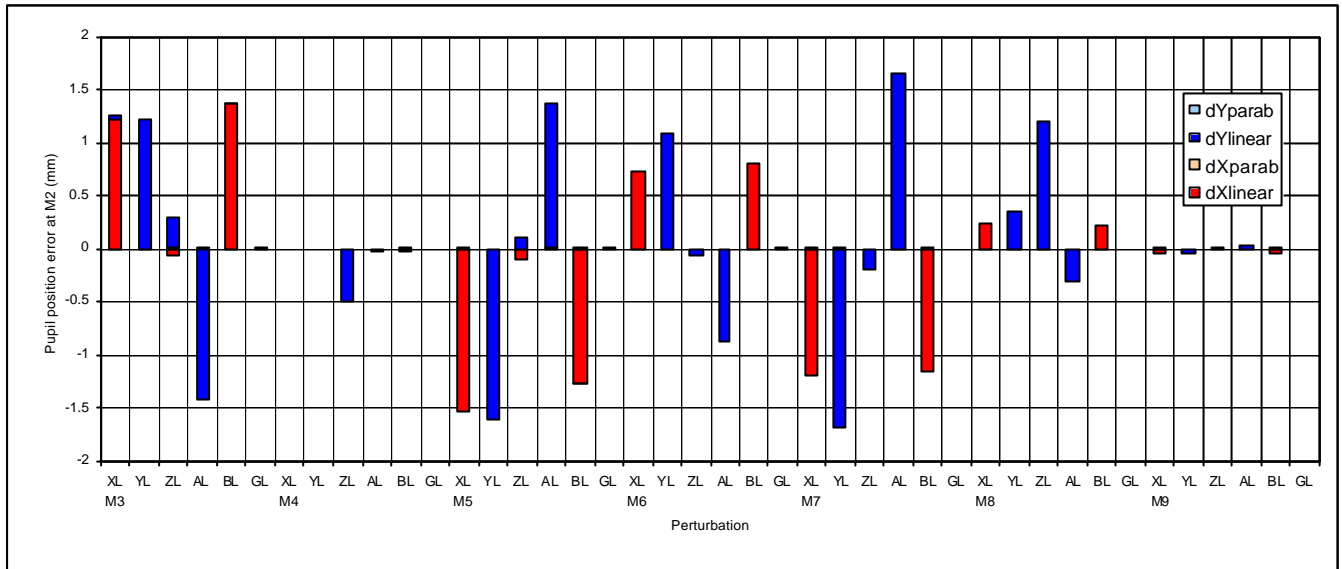


Figure 5. Sensitivity of each photometer mirror to 0.1mm decenter tolerance (XL along x axis, YL along y axis, ZL along z axis) and to 1arcmin rotation tolerance (AL around x axis, BL around y axis, GL around z axis). Apart from M3 and M5, the z axis is perpendicular to each surface at its apex, the y axis is perpendicular to z in the plane of the system, the x axis is perpendicular to y and z. For M3 and M5, the z axis is shifted by 20mm so as to coincide approximately with the centre of gravity of the mirrors, and tilted so as to be perpendicular to the surface at that point.

Results are in mm measured at the M2. For an M2 radius of 150mm, an error  $DR = 1\text{mm}$  corresponds to a fractional pupil alignment error of  $DR/R = 0.67\%$ . Red bars show displacements along the x direction, blue bars along the y direction. Light blue and light red correspond to non-linear sensitivity components: these are clearly insignificant.

Apart from M4 (conjugated with the pupil) and M9 (not involved in pupil imaging since after the cold stop), all mirrors have similar sensitivities. Errors due to GL tilts (azimuth rotation) are very small for all mirrors, the alignment budget is not dimensioning for these perturbations. A tolerance of about 0.5 degrees is probably acceptable to avoid vignetting.

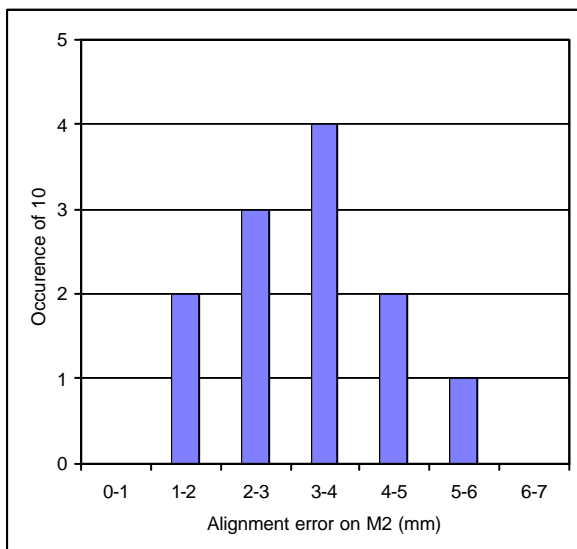


Figure 6. Monte Carlo analysis with 10 randomly generated combinations of alignment errors. Each mirror has been given decenters and tilts up to  $\pm 0.1\text{mm}$  and  $\pm 1\text{arcmin}$  in each direction with an even statistical distribution. The resulting average error is 3.4mm ( $DR/R = 2.2\%$ ) and the 90% percentile is at 4.8mm ( $DR/R = 3.2\%$ ), i.e. less than the 4% RSS assumption made in the error budget (Figure 4). This provides a "confidence margin". [The RSS assumption actually works with standard deviations. Since the standard deviation of an even distribution between  $\pm a$  is  $s = a/\sqrt{3}$ , there is a factor  $\sqrt{3}$  between the Monte-Carlo average and the RSS sum:  $2.2\% \sqrt{3} = 3.8\%$ , compared with 4.0% in the budget.]

<b>LAM</b> <b>LOOM</b>	<b>Projet</b> <b>SPIRE</b>	Herschel - SPIRE: Optical Error Budgets REF : LOOM.KD.SPIRE.2000.002-4	PAGE : 16 / 24 17 Jan 2002
---------------------------	-------------------------------	---	-------------------------------

#### 4. Spectrometer budgets

As of December 2001, corner cubes (CC) have been replaced by roof-top (RT) mirrors in the spectrometer optical design. This allows aligning the detectors with the global instrument axis, which simplifies the mechanical implementation of the detector system. Optical quality is not affected by this change. Alignment tolerances are more severe however in the plane containing the apex of the RT, see sec 4.3.4.

In this document, the change has been implemented only when it is significant. For example, in Sec 4.1, the change in transmission in going from 13 to 12 surfaces has no impact on the total transmission budget. When the change is significant, both CC and RT cases are considered.

##### 4.1. Throughput

In the spectrometer, an exactly-sized aperture stop (referred to as spectrometer cold stop, SCS) is located between SM6 and SM7 in connection with the passage of the beam through the optical bench. An image of this stop exists close to the detectors, between SM11A/B and SM12A/B, but this is not used due to mechanical constraints. Instead, the mirrors SM12A/B will be shaped according to the geometrical beam, playing the role of a partial stop avoiding detectors to see too far into the instrument. For the central detector, this stop will be oversized with respect to the SCS, for edge detectors it will be oversized on one side and exactly sized on the other side.

Similar alignment tolerances as those imposed on the photometer due to pupil alignment are imposed on the spectrometer due to interferogram contrast. A similar level of misalignment may therefore be expected between the two stops within the spectrometer as that calculated for internal alignment in the photometer. Since the stop on SM12A/B is not in a pupil image and sized as described above, the effect on throughput is smaller however and only seen for edge detectors. As a worst case, we have assumed the value given for internal alignment in the photometer budget, Sec. 3.3, ie.  $\Delta R/R = 4\%$ , hence  $T = 1 - 0.64 \Delta R/R = 97\%$ .

Since the SCS is located early in the optical train, we assume the photometer value for external alignment ("Telescope to SPIRE interface" in Sec. 3.3) for its misalignment with the telescope pupil, ie.  $\Delta R/R = 6\%$ , hence  $T = 1 - 0.64 \Delta R/R = 96\%$ .

Pupil aberrations due to the optical design are estimated to  $\Delta R/R = 5\%$ , hence  $T = 1 - 0.64 \Delta R/R = 97\%$ .

Losses due to diffraction and baffling are estimated to 20% (TBC). We have assumed 99% reflectivity of each of 13 mirror surface (CM3 to SM12 plus three CC surfaces) and a total filter and beamsplitter efficiency of 40%.

The throughput loss of 50% due to band-pass filtering is not included (cf BMS).

Horn coupling efficiency is not accounted for, in accordance with IRD-OPTS-R05, neither on-axis nor off-axis. The efficiency for edge detectors was particularly poor in the original design due to the telecentric horn arrangement. Adding field lenses in front of the detectors, as has recently been proposed will improve this at the cost of some absorption and reflection losses. These effects are not included in the budget.



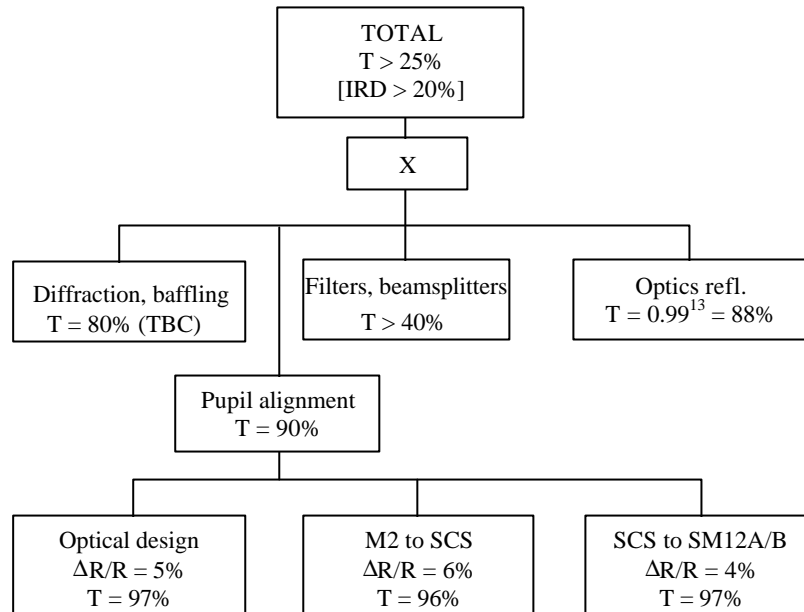


Figure 7. Spectrometer throughput budget.

4.2. Wavefront error

Wavefront error budget meets IRD. See Sec. 3.2 for comments. RMS surface error of 1 μm (2μm WFErms) is assumed for each of 15 reflecting surfaces (CM3 to SM12 plus 3 CC surfaces plus 2 BS surfaces). Transmissive components are not included since their thickness is negligible.

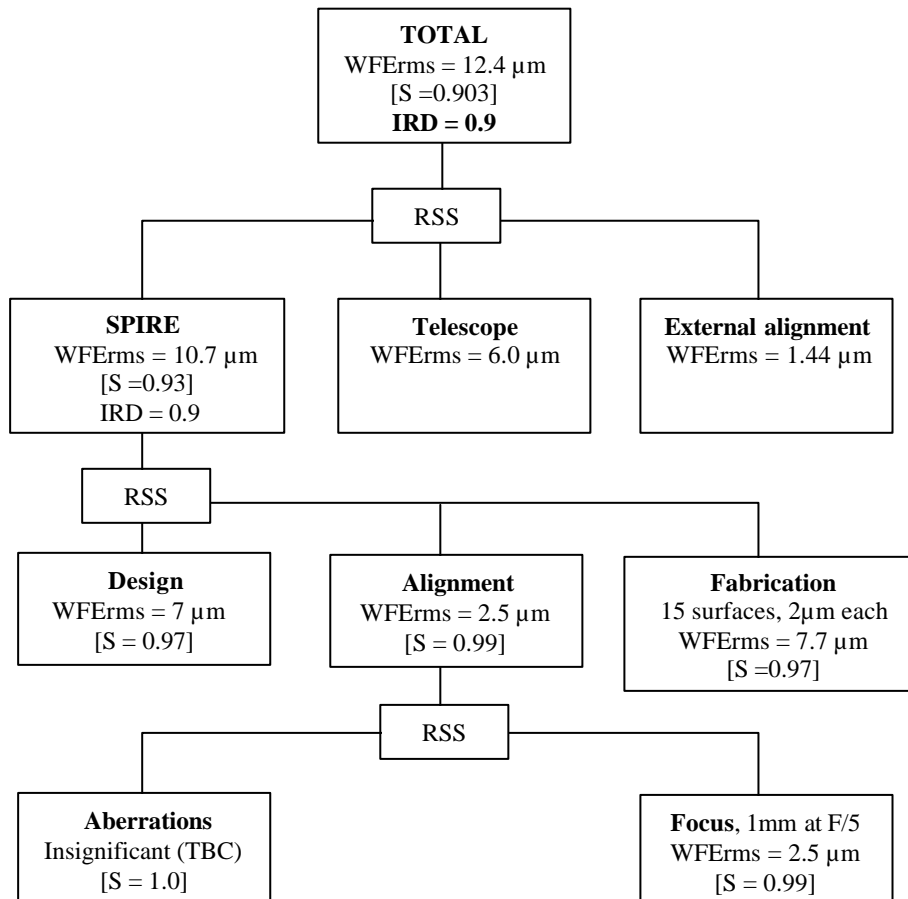


Figure 8. Spectrometer wavefront budget.

<b>LAM LOOM</b>	<b>Projet SPIRE</b>	Herschel - SPIRE: Optical Error Budgets REF : LOOM.KD.SPIRE.2000.002-4	PAGE : 18 / 24 17 Jan 2002
---------------------	-------------------------	---	-------------------------------

### 4.3. Interferogram contrast

Contrast is affected by tilt and shear between the interfering wavefronts and balance between beamsplitter R and T. Tilts and shears are discussed in the following, beamsplitter balance is discussed in sec. 4.3.5.

Interferogram contrast describes the efficiency with which the instrument renders the undulating interference intensity created by the FTS. It is defined for a monochromatic beam as:

$$k = \frac{I_{\max} - I_{\min}}{I_{\max} + I_{\min}} \quad (1)$$

where  $I_{\max}$  and  $I_{\min}$  are maximum (constructive) and minimum (destructive) interference intensities, respectively.

When  $OPD \neq 0$ , wavefronts from an off-axis object are sheared due to geometry, and may be tilted due to differential distortion. Misalignments of components within the interferometer also introduce tilt and shear.

#### 4.3.1. Wavefront tilt

When interfering wavefronts are tilted in the pupil by angle  $q$ , the optical path difference varies across the pupil, i.e. Newton's fringes can be observed. This results in a reduced interferogram contrast which Lambert and Richards [RD2] calculated, for a uniformly illuminated circular (top-hat) pupil function, using the van Cittert Zernike theorem:

$$k_T = 2J_1(u)/u \quad (2)$$

where  $u = pqd/l$  and  $d$  is the diameter of the pupil. It is convenient to quantify the tilt in the pupil in terms of the resulting image shift at the detector:  $D = qf = qFd = 0.038 q$  [arcmin], when  $F = 5$  and  $d = 25$  mm. Then:  $u = pD/(lF)$ . Applying the Taylor expansion to eq. (2) provides an approximation valid for small perturbations:

$$k_T \approx 1 - u^2/8 = 1 - 0.79\Delta^2$$

when  $l = 250\mu\text{m}$  and  $F = 5$ .

In SPIRE, the pupil function is a clipped Gaussian. We have estimated the contrast in this case by numerical calculations. Assuming a Gaussian function clipped by an  $F = 5$  circular aperture at 25% power level (this is conservative since the designed clipping level is  $1/e^2 = 13\%$ ), the contrast function is (figs 9 and 10):

$$k_T \approx 1 - 0.59\Delta^2 \quad (3)$$

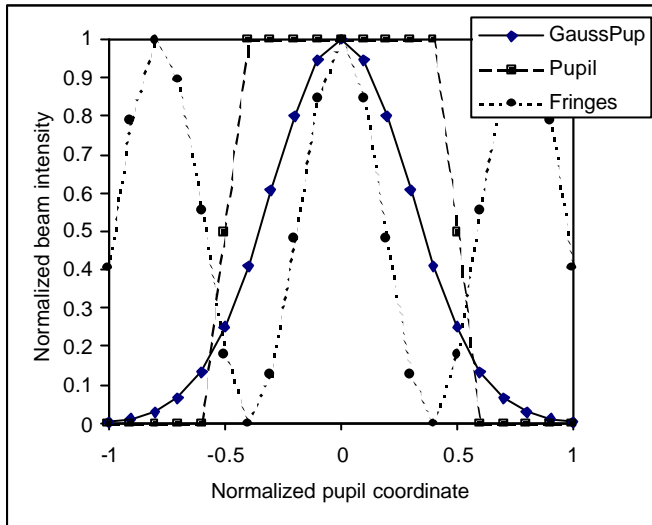


Figure 9. Beam patterns for calculation of wavefront tilt effect. Contrast is lost due to formation of Newton's fringes (dotted).

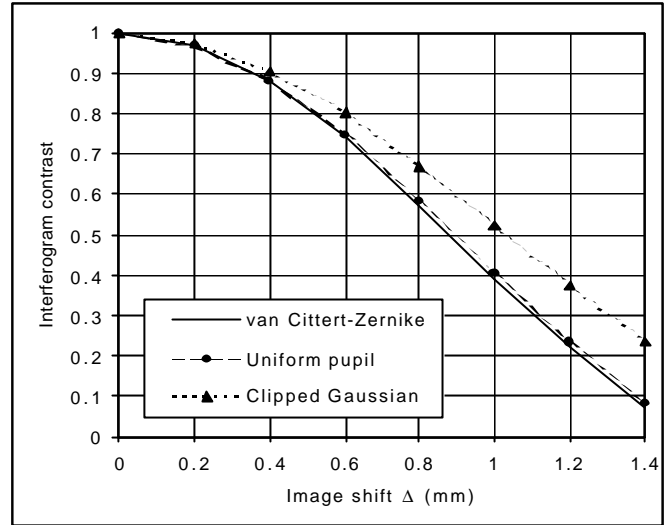


Figure 10. Comparison between contrast for uniform pupil and clipped-Gaussian pupil.

#### 4.3.2. Wavefront shear

When the interfering wavefronts are sheared in the pupil, one must distinguish between coherent and incoherent radiation [RD2]. In the SPIRE case, where the objects under study are generally unresolved, hence coherent, the contrast function equals the MTF of the camera system. The MTF may be calculated as the autocorrelation of the complex pupil function. Assuming perfect optics, which is not far from being the case for SPIRE, the pupil function is real and equal to the pupil transmission function. In the case of a uniform circular pupil, the contrast is therefore given by the classical diffraction limited MTF curve [RD4] and may be expressed as:

$$k_S = (2/\pi)[\text{acos}(u) - u\sqrt{1-u^2}] \approx 1 - (4/\pi)u \quad (4)$$

when  $u$  is small, where  $u = s/d$ ,  $s$  is pupil shear, and  $d$  is the pupil diameter. Note that this function falls off linearly with shear.

Numerical calculations shows that for a Gaussian pupil clipped at 25% power level (conservative as noted above) by a circular aperture of diameter  $d$  (fig. 11), the fall-off is parabolic and approximately equal to (fig. 12):

$$k_S \approx 1 - 3.3 u^2 = 1 - 5.3 \times 10^{-3} s^2 \quad (5)$$

for a pupil of diameter  $d = 25$  mm.

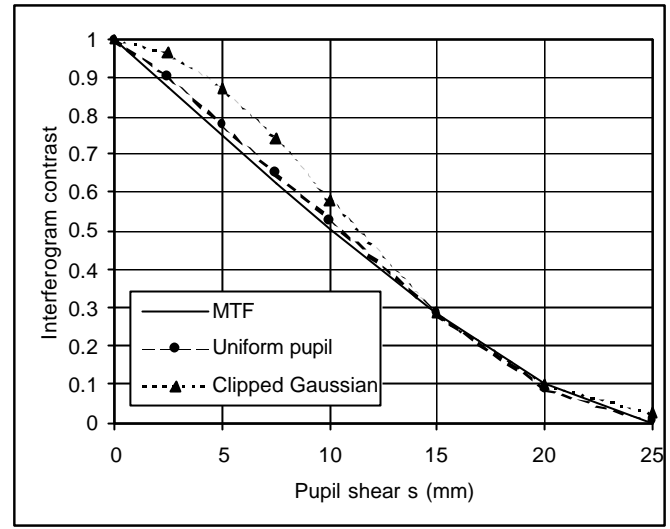
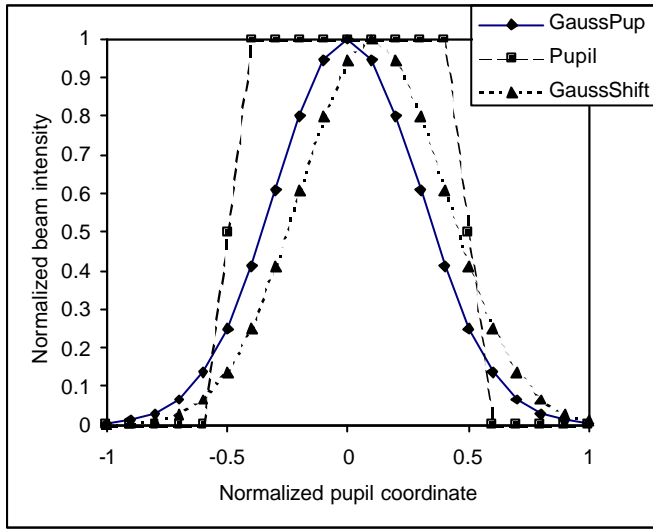


Figure 11. Beam patterns for calculation of wavefront shear effect.

Figure 12. Comparison between contrast for uniform pupil and clipped-Gaussian pupil.

4.3.3. Optical design

Two sources of contrast loss due to optical design are identified:

1) Shear for off-axis object.

As seen in fig. 13, an off-axis beam travelling through a two-beam interferometer at angle  $\beta$  experiences a pupil shear of:

$$s = OPD \sin \beta \approx OPD \beta$$

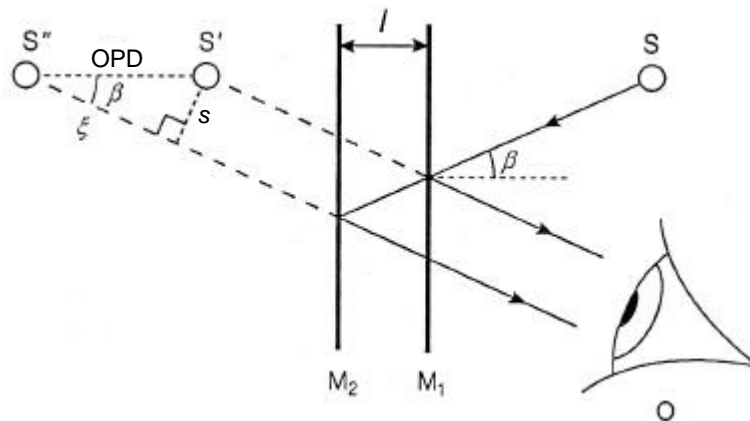


Figure 13. Shear for an off-axis beam in a two-beam interferometer.

The angle  $\beta$  for an object at the edge of the FOV is given by the Lagrange invariant as

$$\beta = FOV D / (2d)$$

where FOV is diameter of the sky field of view and D is the telescope entrance pupil diameter. Assuming FOV = 2.6', D = 3300mm, d = 25mm, we get  $\beta = 2.86^\circ$ . At the nominal resolving power of 100, the

<b>LAM</b> <b>LOOM</b>	<b>Projet</b> <b>SPIRE</b>	Herschel - SPIRE: Optical Error Budgets REF : LOOM.KD.SPIRE.2000.002-4	PAGE : 21 / 24 17 Jan 2002
---------------------------	-------------------------------	---	-------------------------------

maximum OPD is 12.5mm, hence pupil shear is  $s = 0.62\text{mm}$ . At maximum resolving power (1000), the shear is  $s = 6.2\text{mm}$ . Contrasts estimated by eq (5) are 99.8% and 80%, respectively.

## 2) Tilt due to differential distortion.

Since there is powered optics within the interferometer and the OPD scanning causes a longitudinal displacement of the exit pupil, differential aberrations between the two interfering beams may occur. No significant difference in wavefront error has been detected, but a slight difference in distortion causes a shift of the image position (ie wavefront tilt) for off-axis objects. The shift increases linearly with OPD and reaches  $\Delta = 0.04\text{mm}$  at  $R = 100$  and  $\Delta = 0.4\text{mm}$  at  $R = 1000$ . Contrasts estimated by eq. (3) are 99.9% and 90.6%, respectively.

The total theoretical contrast of the optical design is therefore 99.7% at  $R = 100$  and 72.5% at  $R = 1000$ . This is to be compared with results obtained by ASAP analysis.

### 4.3.4. Interferometer alignment

Contrary to optical design losses, alignment losses are independent of OPD and FOV. Tilts and decenters of each component within the interferometer in general introduce both tilts and shears to the interfering wavefronts. Table 1 gives wavefront tilts and shears produced by 0.1mm decenters and 1' tilts of each component within the interferometer. The RSS of tilt and decenter values are calculated, and the total budgets estimated by multiplication with  $\sqrt{2N}$ , where the  $\sqrt{2}$  factor accounts for errors in both x and y directions, and N is the number of components in each case. The total budgets shows fringe contrast in brackets.

Note that alignment of roof tops (RT) is sensitive to tilt only in the plane containing the RT apex, and to shear only in the direction perpendicular to this plane. For this component the factor  $\sqrt{2}$  has therefore been dropped.

Clearly, the most critical components are the collimator and camera mirrors. Any significant reduction in alignment precision of these components will have important impacts on the alignment budget. Beamsplitter and corner cube alignments are far less critical. Tolerances may be relaxed in these cases, this may be particularly interesting for the internal alignment of the corner cubes.

In discussions with Guy Michel and Don Jennings, it became clear that they considered some adjustment capability highly desirable, at least for the qualification model, to allow optimizing cold IR operation. CIRS was originally designed without adjustments, but this was included later and proved useful during "debugging" of the qualification model. It is not clear how this could be realised in SPIRE, but it should be discussed. Don also suggests that the imaging capability of SPIRE may be utilised in the cold alignment check, eliminating the need for "cold fiddling". TBT (=To be thought about :)

**Important note: The current budget concerns the scientific beam. Constraints due to mechanical or sensor concerns may in some cases be overriding.**

<b>LAM LOOM</b>	<b>Projet</b>	Herschel - SPIRE: Optical Error Budgets REF : LOOM.KD.SPIRE.2000.002-4	<b>PAGE : 22 / 24</b>
	<b>SPIRE</b>		<b>17 Jan 2002</b>

Table 1. Wavefront tilt, in terms of image shift  $D$ , and wavefront shear,  $s$ , due to  $1\epsilon$  tilts and  $0.1\text{mm}$  decenters

Component	1 $\epsilon$ tilt		0.1mm decenter		Total per comp, per dimension		Nb of units	Total budgets (contrast)	
	Tilt, $D$ (mm)	Shear, $s$ (mm)	Tilt, $D$ (mm)	Shear, $s$ (mm)	Tilt, $D$ (mm)	Shear, $s$ (mm)		Tilt, $D$ (mm)	Shear, $s$ (mm)
<b>Beamsplitters</b> (SBS1, SBS2)	0.023	0.087	0	0	0.023	0.087	2	0.046 (99.9%)	0.174 (99.98%)
<b>Collimators</b> (SM9A, SM9B)	0.075	0.087	0.1	0.12	0.13	0.15	2	0.26 (96%)	0.30 (99.95%)
<b>Cameras</b> (SM10A, SM10B)	0.075	0.087	0.1	0.12	0.13	0.15	2	0.26 (96%)	0.30 (99.95%)
<b>CC relative</b> <sup>1</sup>	0	0	0	0.2	0	0.2	2	0 (100%)	0.40 (99.92%)
<b>RT relative</b> <sup>1</sup>	0.075	0	0	0.2	0.075	0.2	2	0.11 (99.3%)	0.28 (99.96%)
<b>CC or RT internal</b> <sup>2</sup>	0.038	0	NA	NA	0.038	0	2	0.076 (99.7%)	0 (100%)
<b>CC scan axis</b> <sup>3</sup>	0	0	0	0	0	0	1	0 (100%)	0 (100%)
<b>RT scan axis, constant</b>	0.15	0	0	0	0.15	0	1	0.15 (98.2%)	0 (100%)
<b>RT scan axis, dynamic</b>	0.15	0	0	0	0.15	0	1	0.15 (98.2%)	0 (100%)
<b>Total (CC)</b>								<b>91.6%</b>	
<b>Total (RT)</b>								<b>87.8%</b>	

**Notes:**

- 1) Relative alignment between upper and lower CC vertices or RT apexes. Axial separation is not critical for contrast but should be kept below 1 mm.
- 2) Misalignments of the CC or RT faces which cause  $1'$  beam deviation between input and output beams is assumed.
- 3) Fringe contrast is insensitive to tilts and decenters of perfectly mounted back-to-back corner cubes during the scan. Decenters give pupil movement however, so to avoid vignetting, the decenter should be less than 1 mm, say.

#### 4.3.5. Beamsplitter balance

If interference is formed between two wavefronts of intensity  $I_1$  and  $I_2$ , then the contrast of the interference fringes may be expressed as:

$$k = \frac{2\sqrt{I_1 I_2}}{I_1 + I_2}. \quad (6)$$

In a Mach-Zehnder, dual output configuration with two identical beamsplitters of reflectivity R and transmissivity T, the intensities  $I_1$  and  $I_2$  may be expressed in terms of R and T for each of the two outputs A and B:

$$I_{1A} = I_{2A} = RT, \quad (7)$$

$$I_{1B} = R^2 \quad \text{and} \quad I_{2B} = T^2. \quad (8)$$

By eq. (6) we therefore have:

$$k_A = 1,$$

$$k_B = 2RT/(R^2 + T^2).$$

The A output therefore has 100% contrast regardless of beamsplitter performance. Reading values of R and T off the curves presented by PA at the July 99 PDR [RD3], we find approximate contrast values for the B output, see Table 2. For the budget we have taken the worst-case contrast of 94%, occurring at 190 and 500  $\mu\text{m}$ .

*Table 2. Approximate contrast for the B output.*

$l$ ( $\mu\text{m}$ )	R (%)	T (%)	$k_B$ (%)
190	58	40	93.5
250	51.5	46	99.4
333	54.3	43.9	97.7
500	56	40	94.6
625	46	46	100
1000	26	67	67.5

#### 4.3.6. Budget

Figure 14 shows the interferometer alignment budget. Nominal ( $R = 100$ ) contrast values are shown and  $R = 1000$  values are indicated in brackets. With a total budget of 85.8% for nominal resolving power, the required contrast of 80% is achieved with margin.

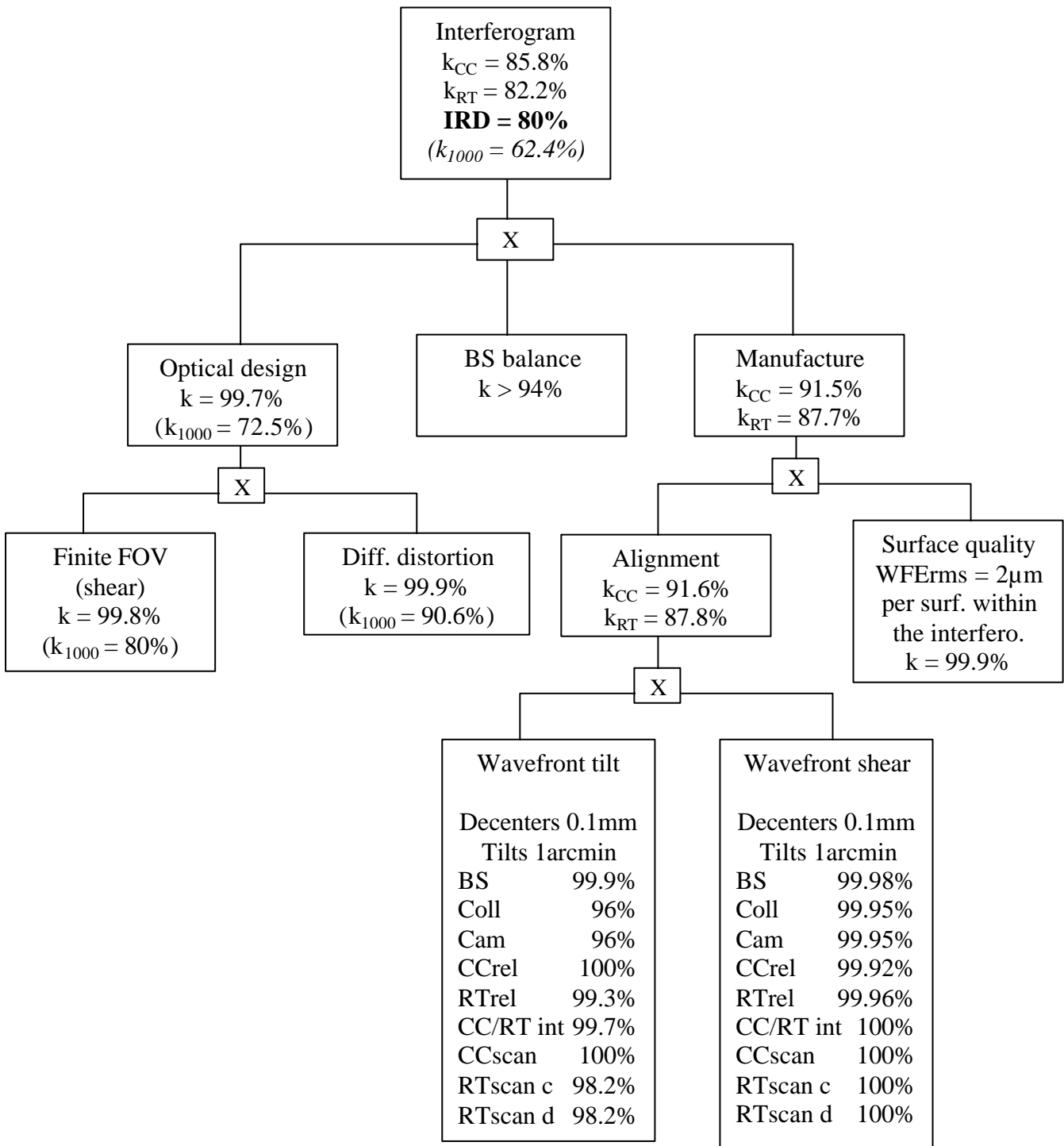


Figure 14. Interferometer alignment budget calculated at 250 µm. Nominal ( $R = 100$ ) contrast values are shown and  $R = 1000$  values are indicated in brackets.